Electromagnetic Simulation of Split-Core Current Transformer for Medium Voltage Applications

N. Paudel[*1], V. Siddharth[1], S. Shaw[1], D. Raschka[1]

ABB Inc., Instrument Transformers & Distribution Components, Pinetops, NC, USA
*Corresponding author: nirmal.paudel@us.abb.com

Abstract: This paper presents the three dimensional (3D) Finite Element Method (FEA) COMSOL model of a submersible split-core current transformer (or sensor) for medium voltage underground vault applications. The model of a single split-core sensor, as well as cross-talk simulation in a three-phase application, is shown. The detail of the COMSOL simulation setup is described. The measurement and simulation results are compared for three different core cross-sections for a full 3D three-phase system including the cable orientations and positions.

Keywords: Split-core transformer, clamp-on current transformer, electromagnetic simulation, submersible current sensor, submersible transformer.

1. Introduction

In the electric distribution network, current and voltage measurement for metering, monitoring, and protection & control applications are done via instrument transformers (current and voltage transformers). These measurement devices are deployed during the construction phase of the electric network. However, it is required on many occasions to replace these devices due to failure or upgrade. Utility companies preferred to replace these devices without any power interruption. For the very same reason, this paper is focused to present a clamp-on current instrument transformer (also called split-core sensor) with split ferromagnetic cores which can be easily installed around the primary conductor without disconnecting the service.

The design is focused to have the low voltage output that is proportional to the current input and, having a very low energy output, minimizes safety concerns associated with open circuited leads on an energized current transformer [1]. The electromagnetic design is performed in COMSOL Multiphysics using the AC/DC Module. The Magnetic Fields physics is coupled with Electrical Circuit interface to perform the FEA & Circuit co-simulation. Since, the split-core transformer is designed for accuracy class of 1% (maximum error <1%) for the entire operating range, the optimal shape of the split-core is investigated through EM simulation.

The simulation was performed for three different core cross-sections. The EM simulation is performed in the Frequency Domain at 60Hz for the wide range of input currents (60A to 4000A) in a single phase configuration and also in 3-phase configurations with each phase separated by 8[in]. The number of turns, wire size, bobbin configuration (angle width), bobbin placements etc. was investigated through various *Parametric Sweep* studies for each of these parameters. The output voltage remains linearly proportional to the input current throughout this operating range as the magnetic core is never saturated due to the two-airgaps in the design [2]. The optimal bobbin angle width was found such that the bobbin when placed next to the air-gaps (on either side) will have the minimum cross-talk (interference) from the other conductor (with & without a sensor in it).

The working principle of the split-core sensor is shown in Figure 1. When the time-varying AC current passed through the primary conductor, the magnetic flux is generated around it. The magnetically permeable core is used to guide and enhance the magnetic flux lines. The time-varying magnetic flux is passing inside the secondary coils, which in turn induces the voltage in each of the secondary coils due to Faradays' law of induction [2]. Since the coils are connected in series along with the load resistor, the induced voltage in each coil is added. The input current in the primary is measured by measuring the proportional voltage induced across the load resistor through the meter or controller as shown in Figure 1.

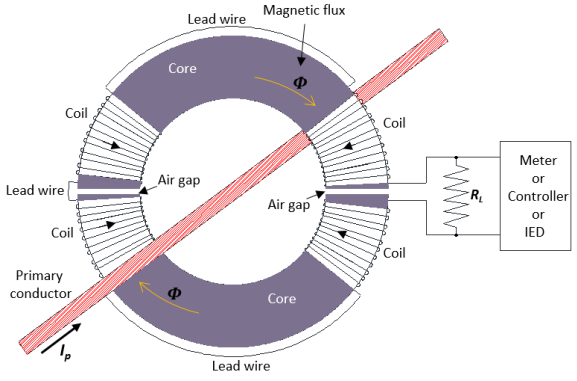

Figure 1: Schematic of the split-core sensor with primary conductor, secondary coils, core, air-gaps and load circuit.

2. Governing Maxwell's Equations

The time-harmonic equations for the *Magnetic Fields* physics in COMSOL is derived from the Maxwell-Ampere's law including the displacement current as:

$$\nabla \times \boldsymbol{H} = \boldsymbol{J} + \frac{\partial \boldsymbol{D}}{\partial t} = \sigma \boldsymbol{E} + \boldsymbol{J_e} + \frac{\partial \boldsymbol{D}}{\partial t} \quad (1)$$

In the above equations, $\mathbf{J}_e$ is the external current density or a current source. This is usually applied through *Coil* features. For time-harmonic fields, the magnetic flux density, **B** and electric field **E** are defined as in terms of the magnetic vector potential, **A** as

$$\boldsymbol{B} = \nabla \times \boldsymbol{A} \quad (2)$$

$$\boldsymbol{E} = -j\omega \boldsymbol{A} \quad (3)$$

Now, combining the above two equations with the constitutive relationships

$$\boldsymbol{B} = \mu_0(\boldsymbol{H} + \boldsymbol{M}) \quad (4)$$

$$\boldsymbol{D} = \epsilon_0 \boldsymbol{E} \quad (5)$$

the Ampere's law for time-harmonic applications becomes

$$(j\omega\sigma - \omega^2\epsilon_0)\boldsymbol{A} + \nabla \times (\mu_0^{-1}\nabla \boldsymbol{A} - \boldsymbol{M}) = \boldsymbol{J_e} \quad (6)$$

This is the governing equation that is being solved when *Magnetic Fields* physics is used in *Frequency Domain* in COMSOL Multiphysics. In addition, to obtain a unique solution, the explicit gauge called *Coulomb gauge* is applied via the equation

$$\nabla \cdot \mathbf{A} = 0 \quad (7)$$

The above equation is implemented in COMSOL by adding the *Gauge Fixing for A-Field* feature within the *Magnetic Fields* physics.

3. Geometry

In order to set up an efficient finite element model, it is a good practice to always look for the options to simplify the model geometry. Not all the geometrical details are needed for EM simulations. For example, in the single sensor setup, we only considered the model with materials such as magnetic core, copper conductor and copper coils (see Figure 2). All other insulating materials/parts such as plastic bobbins, polycarbonate outer casing, and polyurethane filler etc. are not included for EM simulation.

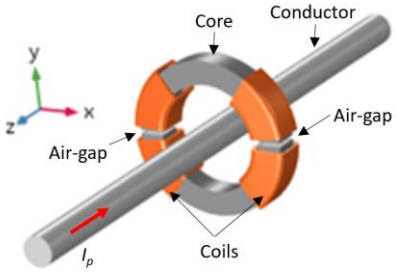

Figure 2. Configuration of split-core CT depicting primary conductor, secondary coils, core, and air-gaps.

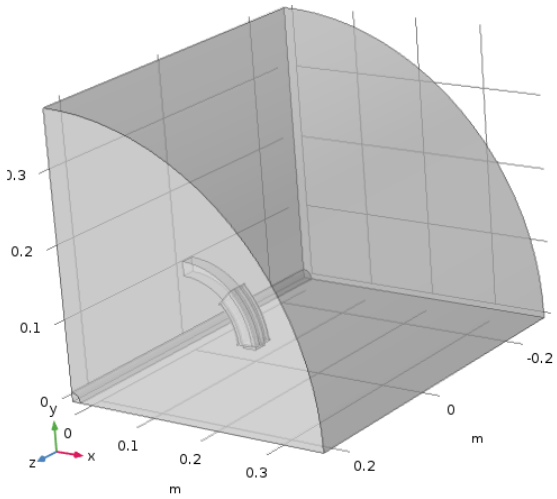

Figure 3: Quarter geometry of split-core sensor used for simulation.

In addition, the options for geometrical symmetry and physics symmetry is explored to further reduce the size of the FEA model. In this single sensor model, only the quarter model is considered exploiting the symmetry in two different planes (*xz* and *yz*) as shown in Figure 3. The geometry is fully parameterized. The number of turns in secondary windings, wire gauge, the coil fill factor, core cross-section, core radius, etc. are parameterized. An uneven wire distribution on the inner and outer side of the bobbin as depicted in Figure 4 is also considered in the model geometry.

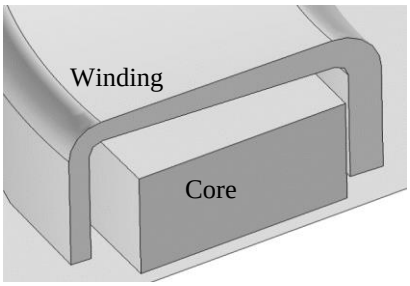

Figure 4: Geometry of uneven wire distributed winding around a toroidal air-gaped core. Bobbin is not shown here.

4. Physics & Boundary Conditions

The *Magnetic Fields* physics is used in *Frequency Domain* to perform the EM simulation of this split-core sensor. The default Ampere's Law feature is used for air and other insulation regions (not shown in the geometry). The *Coil* feature is used to model the primary conductor and secondary coils. Separate Ampere's Law node is used for core domains where the anisotropic conductivity and permeability are assigned.

The primary conductor is modeled as a *Solid conductor* using *Coil* feature. The default copper material properties are used from COMSOL Material library. Since only a quarter section of the primary conductor is model, this factor is included under Geometry Analysis sub-node as Coil area multiplication factor (F_A = 4). The primary conductor is excited with current parameter (I_p) which was varied from 60A to 600A during the simulation. The *Input* and *Output* sub-features were applied on the opposite sides of the primary conductor. On the two symmetry cut planes of the primary conductor, the *Perfect Magnetic Conductor* boundary condition is used.

The secondary coils are modeled as *Homogenized multi-turn* using the *Coil* feature. Since there exist symmetry in the placement of four secondary bobbins, only one is modeled via *Coil* feature. The *Input* sub-feature is applied to the internal cross-section of the coil, no *Output* sub-feature is needed here. This secondary coil is connected with the load resistor (R_L). In a real application, the voltage across the load resistor is measured via a standard meter or controller or relay. The input impedance of the measuring device (R_m= 1Mohm) is also included in the simulation. This is connected in parallel to the load resistor across which the voltage is measured. In this particular sensor, the design target is to obtain 10V across this load resistor when the primary current is 600A.

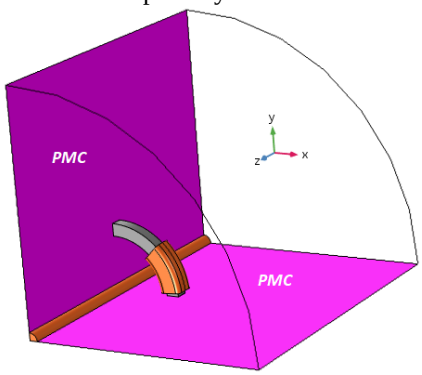

Figure 5. Illustration of quarter model of split-core CT.

The *Perfect Magnetic Conductor* boundary condition $\mathbf{n} \times \mathbf{H} = 0$ is imposed (as shown in Figure 5) where the tangential component of a magnetic field and also the surface current density is zero. This condition is used on the exterior boundaries to specify the symmetry condition for electric fields and electric currents. The rest of the external boundaries is default *Magnetic Insulation* boundary condition.

Modeling of the Laminated Core

Since the magnetic simulation will be performed in the Frequency Domain, the nonlinear magnetic BH curve (DC magnetization) cannot be directly used. It must be converted to an equivalent AC effective BH Curve. The DC magnetization curve is converted into effective BH Curve using the Effective Nonlinear Magnetic Curves Calculator App from COMSOL Application Library. This effective BH curve is then used in modeling the magnetic core.

During the simulation of a single split-core sensor, it was found that the magnetic permeability of the core for the operating range from 60A to 600A remains almost constant. This is due to the fact that the value of magnetic flux density is very low in the core and the core is operating at much less flux density value than the nonlinear saturation level. The two air-gaps in the core also helps to lower the magnetic flux level in the core [2]. With this finding, the simulation of three-phase systems with varying conductor diameter, sensor offset, coil positioning, and cable orientations is done by just considering a linear magnetic material with relative permeability (μ_r=26400) value obtained from the single split-core sensor simulation.

To model the laminated core (two halves), the lumped approach is used. Instead of explicitly modeling each laminated sheets and insulation in between, the lumped anisotropic (diagonal matrix) conductivity and permeability values were used [3]. The new cylindrical coordinate system (as shown in Figure 6) is defined with a center of the core as the origin and the conductivity and magnetic permeability were defined with reference to this cylindrical coordinate system.

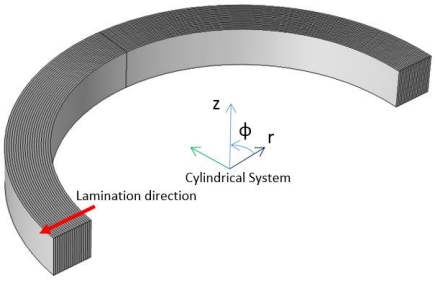

Figure 6: Geometry of M4 steel core showing cylindrical coordinate system and lamination direction.

$$\begin{bmatrix} \sigma_r & & \\ & \sigma_\emptyset & \\ & & \sigma_z \end{bmatrix} = \begin{bmatrix} \frac{\sigma_c}{1000} & & \\ & \sigma_c & \\ & & \sigma_c \end{bmatrix} \quad (8)$$

$$\begin{bmatrix} \mu_r & & \\ & \mu_\emptyset & \\ & & \mu_z \end{bmatrix} = \begin{bmatrix} \frac{\mu_c}{1000} & & \\ & \mu_c & \\ & & \mu_c \end{bmatrix} \quad (9)$$

where, $\sigma_c = 1.9608\ [S.m^{-1}]$ is the core electrical conductivity and $\mu_c = 26400$ is the relative permeability of the linearized effective BH curve of the M4 steel core.

5. Single Sensor Simulation

During the development of this split-core CT, various core configurations have experimented, for example, rectangular, circular, and I-core. However, the circular core was found to be most suitable during the initial study. The difficulty of winding on the half circular core was overcome by using angular shaped small bobbins to make part coils. These coils are connected in series to achieve required secondary turns. These bobbins can be slipped on a core to make one complete coil for one half of core. The jumper wire is used to connect the two halves of the bobbins. Finally, the series connection of these four coils is series connected with the load resistor across which the voltage is measured.

For circular core, three different core cross-sections, as shown in Figure 7, were analyzed. The single sensor simulation with Core B was performed to compare the number of turns vs output voltage across the load resistor. Table 1 demonstrates the interesting result for the same based on the configuration of Figure 2. By increasing the number of turns in each coil from 4000 to 6000, keeping the bobbin sector size fixed, the induced voltage across the load resistor is decreasing. This seems to be counter-intuitive. However, this is because of the fact that the internal resistance of the coil increased by increasing the number of turns and become comparable to the load resistor. Due to the internal voltage drop in the coil resistance, less voltage is showing up in the load resistor. The simulation was a powerful tool to understand this counter-intuitive phenomenon. This clearly demonstrates the importance of the FEA and load circuit co-simulation in the design process. As expected, the open circuit voltages increased with an increase of a number of turns, but when the load resistor is connected, the voltage drop across the R_L decreased at the same time the voltage drop on the internal resistance of coil somewhat remains constant. This simulation result was used to prototype the sample with 6000 turns secondary that provided around 10V across the load resistor. The final tuning was done by slightly adjusting the load resistor.

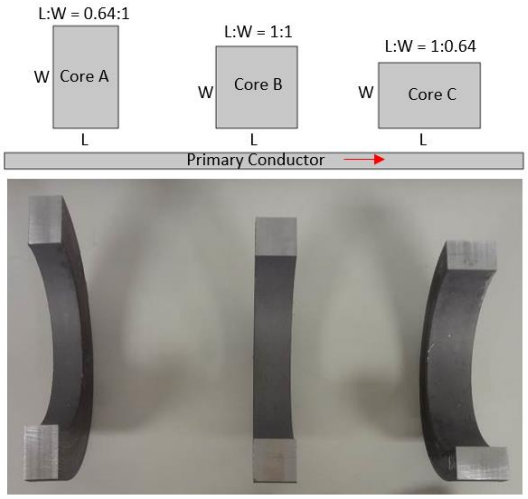

Figure 7. Cross-sections of three circular cores (top) and their respective pictures showing only halves (bottom).

Table 1: Simulation results of voltages (V) while varying the number of turns in secondary coil with and without R_L.

Number of turns	Voltage drop in coil resistance	Voltage across R_L	Open circuit voltage
4000	19.138	15.337	130.5
4500	19.486	13.774	146.99
5000	19.771	12.482	163.36
5500	20.015	11.402	179.7
6000	20.237	10.489	196.17

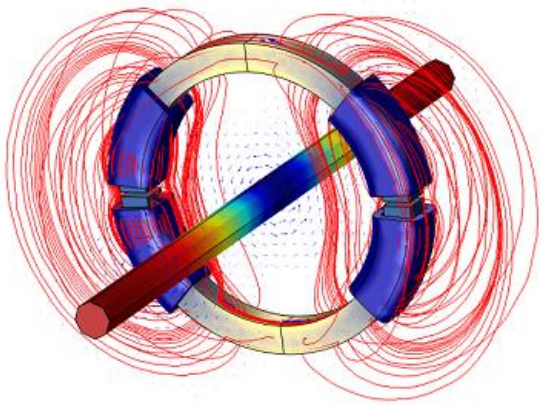

Figure 8. Result depicting magnetic flux density in the core and current density in the primary conductor and coils.

The simulation was also performed for configuration in which all four bobbins were away from the air-gaps as shown in Figure 9. It was found that this configuration was less preferable compared to the one shown in Figure 2 due to more cross-talk. The cross-talk for this configuration when Core B was used was more than >2%, therefore, not suitable for this split-core sensor to meet 1% accuracy.

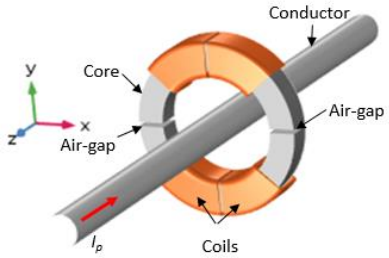

Figure 9: Sensor configuration in which the bobbins are away from the air-gaps.

6. Three-phase Cross-Talk Simulation

After the simulation of a single split-core sensor was completed, the analysis was extended for three-phase configuration. In the three-phase study, the sensors were placed in a horizontal fashion similar to the underground vault application configuration in the electric utilities. The separation between the corresponding phases was only 8 inches. For EM simulation, the geometrical symmetry was explored and only a quarter model of a three-phase system was modeled as shown in Figure 10. In this setup, all four bobbins of the secondary coils were placed close to the air-gaps.

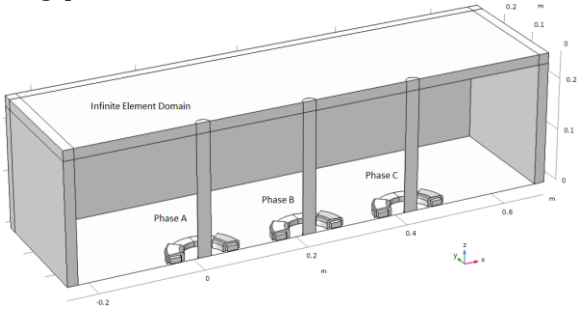

Figure 10: Quarter geometry of a 3-phase setup depicting sensors and infinite element domain around.

To minimize the number of mesh elements, the meshing was customized. In the primary conductors and infinite element domains, the swept mesh was used. In the rest of the geometry, triangular & free tetrahedral mesh was used with different sizes. The maximum value of the mesh size in a core was set to be the half of the skin depth in the core. The skin depth in the core was computed in the parameter section based on the operating frequency (60Hz), electrical conductivity and the linearized effective relative permeability from the single sensor simulation. The finalized mesh for the simulation is shown in Figure 11.

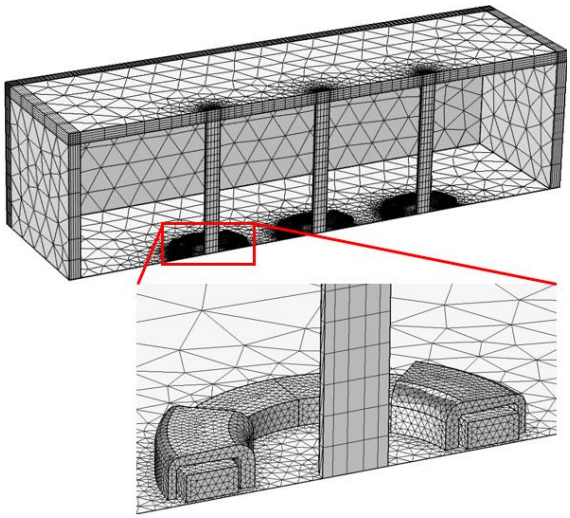

Figure 11: Quarter geometry of a 3-phase setup depicting sensors and infinite element domain around (top). The zoom-in view of mesh around coils and core (bottom).

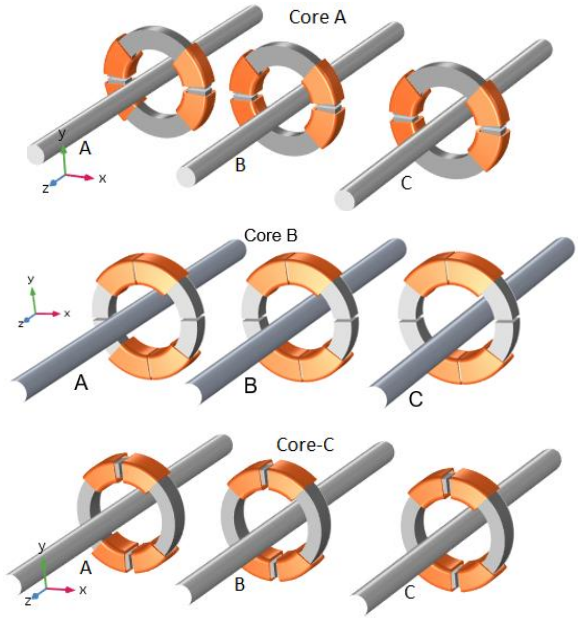

Figure 12: Core size, conductor position and sensor orientation combinations studied for cross-talk simulation.

Notice that the three-phase cross-talk configurations shown in Figure 12 are different not only in the type of core used but also on how the secondary coils are arranged and the air-gap is aligned with the corresponding three phase conductors. Combination of many possible simulation studies was conducted for understanding the cross-talk when one or several sensors are offsets from its original position. The voltage induced in the mid sensor when only phase B was excited was taken as the reference system to calculate the error in the simulation. The voltage induced on each of these sensors are calculated and compared with the reference. Only the result for

voltage induced in the sensor placed in phase B (configuration in Figure 12-middle one) is shown in Figure 13 and Figure 14. The current in phase B was excited all the time, but the current in phase A and C were excited alternatively and finally, all phases were excited together as shown these figures.

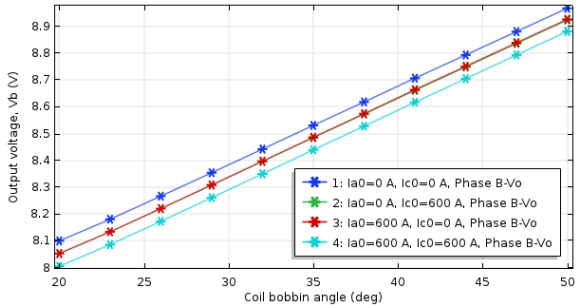

Figure 13: Output voltage of sensor placed in phase B with Core-B used and when the coils in secondary are placed away from the air-gaps.

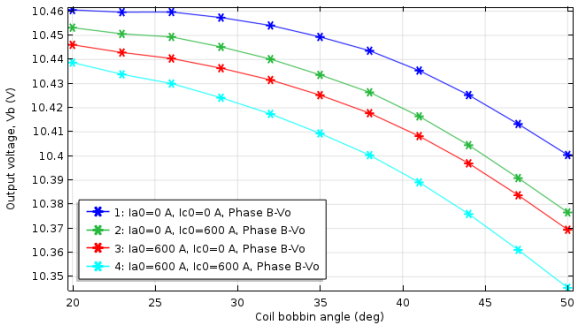

Figure 14: Output voltage of sensor placed in phase B with Core-B used and when the coils in secondary are placed next to the airgaps.

It was verified experimentally and through simulation that the core with the square cross-section (Core B) demonstrate the best performance in terms of the accuracy spread and also cross-talk errors including the sensor position and primary conductor orientation. The details of the simulation setup for the three-phase cross-talk is described in section 6. All the measurements were taken at 60Hz using the PA4000 standard meter from Tektronics. The comparison of the measurement and COMSOL simulation results are shown in Table 2.

Table 2: Simulation and experimental results the cross-talk on different core cross-section design.

Features	Methods	Core A	Core B	Core C
Accuracy Spread/Range	Measurements	0.90%	0.60%	0.30%
	Simulations	0.80%	0.56%	0.42%
Cross-talk error (position & orientation)	Measurements	1.10%	0.80%	1.30%
	Simulations	1.20%	0.91%	1.25%

7. Tests & Productization

A split-core CT design is hermetically sealed within a durable, waterproof plastic housing and insulated and protected with polyurethane (PUR). The core and winding are fully protected from the outdoor environment and from storm waters up to 2m deep. The enclosure is NEMA Type 6P/IP68W compliant. The measurement accuracy error is guaranteed to be less than 1% in operating conditions with influences from cross-talk and/or for offsets from the center of the primary cable.

The product has been tested for power frequency test voltage of 4[kV] and lightening-impulse test of 10[kV]. The sensor is capable to withstand a rated continuous thermal current of 1.2[kA], rated short-time thermal current of 12[kA] for 1[s], and rated dynamic current of 32.4[kA]. The sensor also incorporated the voltage clipping circuitry which limits output voltage to 65[V], avoiding potential damage to the connected devices during the fault current scenarios. The sensor is a UL Recognized Component (file #E96461). This sensor is also compatible with meters and controllers that accept a nominal input voltage of 10[V] for current measurement. This has been tested and is compatible with S&C 5802, S&C IC2000, and SEL 734B controllers. The split-core sensor was tested as per IEEE C57.13-2016 [5], IEEE 495-2007 [6]. The product was released in 2017 and is commercially available. The final ratings and the photograph for this split-core sensor are shown in Table 3 and Figure 15 respectively.

Table 3: Ratings for the split-core sensor (RSS-1) [4].

Rated primary current	600 [A]
Rated extended primary current	1200 [A]
Rated secondary voltage	10 [V]
Accuracy class	1%
Insulation class	600 [V]
Maximum system voltage	0.66 [kV]
Rated frequency	60 [Hz]
Power frequency test voltage	4 [kV]
Lightning-impulse test voltage	10 [kV]
Rated continuous thermal current	1200 [A]
Rated short-time thermal current	12 [kA]
Duration of rated short-time thermal current	1 [s]
Rated dynamic current	32.4 [kA]
Dimensions	192x172x54
Weight	4.5 [kg]
Cable length of electronic transformer	22.9 [m]

Figure 15. Picture of a final product of the submersible split-core sensor (RSS-1) installed in the test setup.

8. Conclusions

This paper outlines the 3D simulation of a split-core current transformer for underground submersible applications. It is shown that the optimal circular core with square cross-section perform best to achieve the measurement error less than 1% including the cross-talk, sensor offsets, and cable orientations. The AC/DC Module was used to perform the simulation for a single transformer as well as the simulation of the full three-phase system. Finally, the results from the experiment as well as the simulation studies are shown. Simulation reduced design and prototype iterations and help to include design changes for improving performance parameter.

References

[1] R. Mullikin, "Instrument transformer," in Electric *Power Transformer Engineering*, J. H. Harlow, Ed. CRC Press LLC, 2004.

[2] ABB Inc., Instrument Transformers: Technical Information and Application Guide. Retrieved from: https://library.e.abb.com/public/e2462bd7f816437ac1256f9a007629cf/ITTechInfoAppGuide.pdf

[3] H. Neubert et al., "Homogenization Approach for Laminated Magnetic Cores using the Example of Transient 3D Transformer Modeling," COMSOL Conference in Rotterdam, 2013.

[4] ABB Inc., "Type RSS-1 submersible current sensor," Retrieved from: https://search.abb.com/library/Download.aspx?DocumentID=1VAP500010-DB&LanguageCode=en&DocumentPartId=&Action=Launch

[5] IEEE C57.13-2016- IEEE Standard Requirements for Instrument Transformers, 2016.

[6] IEEE 495-2007- IEEE Guide for Testing Faulted Circuit Indicators, 2007.